MDPI

Review

Future Long-Baseline Neutrino Experiments

Francesco Terranova [1,2]

1   Dipartimento di Fisica "G. Occhialini", Università di Milano Bicocca, 20126 Milan, Italy;
    francesco.terranova@cern.ch
2   Istituto Nazionale di Fisica Nucleare (INFN), Sez. di Milano Bicocca, 20126 Milan, Italy

Abstract: Long-baseline neutrino experiments represent the optimal platforms for probing the lepton Yukawa sector of the Standard Model, and significant experiments are either under construction or in the planning stages. This review delves into the scientific motivations behind these facilities, which stem from the pivotal 2012 discovery of the θ_{13} mixing angle. We provide an overview of the two ongoing projects, DUNE and HyperKamiokande, detailing their physics potential and the technical hurdles they face. Furthermore, we briefly examine proposals for forthcoming endeavors and innovative concepts that could push beyond conventional Superbeam technology.

Keywords: neutrino oscillation; accelerator neutrino beams; neutrino masses; mixing

1. Introduction

Long-baseline accelerator neutrino experiments involve the production of neutrinos through the decay in flight of light mesons, such as pions or kaons. These experiments typically utilize powerful proton accelerators that direct high-energy protons at a solid or liquid phase target [1]. The resulting particles are then focused into a decay tunnel, where they generate muon neutrinos primarily through the two-body decays of $\pi^+ \to \mu^+ \nu_\mu$ and $K^+ \to \mu^+ \nu_\mu$ or the corresponding decays of negatively charged mesons. This creates an intense beam of muon neutrinos that travels unimpeded in the forward direction after exiting the tunnel. The tunnel axis, which aligns with the neutrino beam axis, points directly at the neutrino detector, while the distance between the tunnel and the detector is referred to as the facility's *baseline* (L).

Long-baseline experiments can take advantage of facilities with baselines ranging from hundreds to thousands of kilometers, limited only by the size of the Earth itself. This is because neutrinos have a tiny interaction cross-section and can pass through the Earth's surface with minimal beam losses. However, these experiments do face a significant reduction in flux, as the neutrino flux at the detectors decreases as L^{-2}.

The neutrino beam also includes electron neutrinos that originate from the $K^+ \to e^+ \pi^0 \nu_e$ decays of charged kaons or the decay-in-flight of muons inside the tunnel. Long-baseline beams can be enriched in either ν_μ or $\bar{\nu}_\mu$ by changing the magnet polarity of the focusing system. For instance, a neutrino beam where focusing is achieved by a magnetic horn can reverse the horn polarity focusing π^- and defocusing π^+. In this case, the neutrino beam will be rich of $\bar{\nu}_\mu$ originating from the $\pi^- \to \mu^- \bar{\nu}_\mu$ and depleted from ν_μ originating from the $\pi^+ \to \mu^+ \nu_\mu$. If the neutrino detectors can distinguish the neutrino flavor, they will measure the number of neutrinos after oscillations along the beamline L. For a neutrino-enriched run, the detector will measure the oscillation probability $P(\nu_\mu \to \nu_e)$ and $P(\nu_\mu \to \nu_\tau)$, together with the survival probability $P(\nu_\mu \to \nu_\mu)$. Similarly, after an antineutrino-enriched run, we can measure the CP conjugate probabilities of the neutrino-enriched run: $P(\bar{\nu}_\mu \to \bar{\nu}_e)$ and $P(\bar{\nu}_\mu \to \bar{\nu}_\tau)$, and the CPT conjugate of the neutrino disappearance probability: $P(\bar{\nu}_\mu \to \bar{\nu}_\mu)$. All these measurements, however, rely on a precise knowledge of the neutrino flux and flavor at the end of the decay tunnel, which corresponds to the initial un-oscillated flux. Measurements of these initial conditions are provided by

neutrino detectors located just after the decay tunnel and are called *near detectors*. The baseline of the near detectors is of the order of hundreds of meters and, therefore, standard oscillations are negligible. The size of the detectors located at the long baseline L (*far detector*) is usually much larger than the size of the near detector because the far detector must compensate for the L^{-2} flux loss. It is customary to employ the same technologies for both the near and far detectors so that detector systematics cancel at leading order.

After the completion of the CNGS program based on OPERA [2], all current long-baseline experiments are only capable of observing ν_e and ν_μ, together with their antiparticles. As a consequence, the observables of long-baseline experiments are the following oscillation probabilities:

$$\begin{aligned}
\nu_\mu &\to \nu_e \ (\nu_e \ \text{appearance}) \\
\overline{\nu}_\mu &\to \overline{\nu}_e \ (\overline{\nu}_e \ \text{appearance}) \\
\nu_\mu &\to \nu_\mu \ (\nu_\mu \ \text{disappearance}) \\
\overline{\nu}_\mu &\to \overline{\nu}_\mu \ (\overline{\nu}_\mu \ \text{disappearance}) \ .
\end{aligned} \tag{1}$$

As a result, long-baseline facilities have access to a limited set of observables, a restricted range of L, and a relatively narrow range of neutrino energies E, as accelerators primarily produce muon neutrinos from 100 MeV to 100 GeV. When neutrino oscillation parameters were still unknown, there was skepticism about the feasibility of utilizing these facilities to explore the neutrino Yukawa sector of the Standard Model. However, the situation changed dramatically between 2002 and 2012, and long-baseline beams are now considered the most effective tool for investigating this sector.

In this review, we will discuss the significance of long-baseline facilities in investigating the neutrino Yukawa sector, particularly focusing on the discovery of θ_{13} and its implications (Section 2). The discovery of θ_{13} sparked an ambitious experimental program that led to the development of HyperKamiokande (HK) and DUNE (Sections 3 and 4, respectively). Furthermore, we will explore the limitations of current long-baseline experiments and explore potential avenues for future progress (Section 5). We do not discuss other experimental approaches, e.g., based on reactor or atmospheric neutrinos, which can also access some of these oscillation parameters [3,4].

2. Neutrino Physics with Long-Baseline Beams

The Yukawa sector of the Standard Model (SM) is responsible for generating and mixing fermion masses. This sector is described by complex matrices that represent the coupling between the Higgs field and matter fields through Yukawa couplings [5]. Unlike vector bosons, the Higgs mechanism does not provide any predictions about the size of the Yukawa couplings. As a result, the masses of elementary fermions and the mixing between mass and gauge eigenstates are not constrained. To express this sector in terms of physical quantities, we introduce three mass eigenstates for neutrinos (m_1, m_2, and m_3), three mixing angles (θ_{13}, θ_{23}, and θ_{12}), and a CP violating phase (δ). In the Standard Model, neutrinos are described as Dirac fields, so only one complex phase is needed to describe lepton mixing. However, some extensions of the Standard Model consider neutrinos as Majorana particles, which require the introduction of two additional phases (e.g., see Chapter 6 in [6]). These phases cannot be measured by oscillation experiments and, hence, the discussion below is still applicable in the presence of Majorana neutrinos.

The minimal extension of the SM that accommodates massive neutrinos is what is now called the Standard Model even if the SM, in its original formulation, employed massless neutral elementary fermions. Such an extension became mandatory after 1998, when oscillation data demonstrated the massive nature of neutrinos [7]. In the minimally extended SM, massive neutral leptons are treated as (massive) quarks. Their flavor eigenstates are linear combinations of mass eigenstates and the linear operator that mixes the flavor and mass eigenfunctions is a 3×3 complex matrix. In the quark sector, this matrix is called the Cabibbo–Kobayashi–Maskawa (CKM) matrix. The corresponding matrix in the neutrino

sector is the Pontecorvo–Maki–Nakagawa–Sakata (PMNS) matrix $U_{\alpha,i}$. The α index runs over the flavor eigenstates ($\alpha = e, \mu, \tau$) and the i index runs over the mass eigenstates $i = 1, 2, 3$. The only active neutrino fields in SM are left-handed chirality flavor fields $\nu_{\alpha L}(x) \equiv \nu_\alpha$ and

$$\nu_\alpha = \sum_i U_{\alpha i} \nu_i . \tag{2}$$

Here, we dropped the dependence of the field on space–time and the subscript L. It is important to note that in the (minimally extended) SM only fields with left-handed chirality (ν_L) appear in the charged currents (CCs) that describe the coupling of fermions with the $W^\pm$ bosons. The minimally extended SM Lagrangian is built by applying the quark formalism to neutrinos and, hence, neutrinos are Dirac particles. As for the CKM, the PMNS matrix is unitary ($U^\dagger U = \mathbb{I}$) and can be parameterized [5] by three angles and one complex phase. The parameterization that has been adopted for the PMNS locates the complex phase in the 1–3 sector, i.e., in the rotation matrix between the first and third mass eigenstates:

$$
\begin{aligned}
U &= \begin{pmatrix} 1 & 0 & 0 \\ 0 & c_{23} & s_{23} \\ 0 & -s_{23} & c_{23} \end{pmatrix} \begin{pmatrix} c_{13} & 0 & s_{13}e^{-i\delta_{\text{CP}}} \\ 0 & 1 & 0 \\ -s_{13}e^{i\delta_{\text{CP}}} & 0 & c_{13} \end{pmatrix} \begin{pmatrix} c_{12} & s_{12} & 0 \\ -s_{12} & c_{12} & 0 \\ 0 & 0 & 1 \end{pmatrix} \\[2mm]
&= \begin{pmatrix} c_{12}c_{13} & s_{12}c_{13} & s_{13}e^{-i\delta_{\text{CP}}} \\ -s_{12}c_{23} - c_{12}s_{13}s_{23}e^{i\delta_{\text{CP}}} & c_{12}c_{23} - s_{12}s_{13}s_{23}e^{i\delta_{\text{CP}}} & c_{13}s_{23} \\ s_{12}s_{23} - c_{12}s_{13}c_{23}e^{i\delta_{\text{CP}}} & -c_{12}s_{23} - s_{12}s_{13}c_{23}e^{i\delta_{\text{CP}}} & c_{13}c_{23} \end{pmatrix} .
\end{aligned}
\tag{3}
$$

In Equation (3), the three rotation angles are labeled $\theta_{13}, \theta_{23}, \theta_{12}$, and $c_{ij} \equiv \cos\theta_{ij}$ and $s_{ij} \equiv \sin\theta_{ij}$. In this parameterization, $\theta_{ij} \in \left[0, \frac{\pi}{2}\right]$ and $\delta_{\text{CP}} \equiv \delta \in [0, 2\pi]$. Physical observables are independent of parameterization, ensuring that the range of angles and the choice of the complex phase in the 1-3 sector can be made without loss of generality.

All these parameters can be measured by neutrino oscillation experiments except for an overall neutrino mass scale. The neutrino oscillation probability between the two flavor eigenstates $P(\nu_\alpha \to \nu_\beta)$ is the probability of observing a flavor β in a neutrino detector located at a distance L from the source. The source produces neutrinos with flavor α and energy E. The oscillation probability in Natural Units (NUs) is given by

$$
\begin{aligned}
P(\nu_\alpha \to \nu_\beta) = {}& \delta_{\alpha\beta} - 4 \sum_{i<j} \text{Re}\left[U_{\alpha i} U_{\beta i}^* U_{\alpha j}^* U_{\beta j}\right] \sin^2\left(\frac{\Delta m_{ji}^2 L}{4E}\right) \\
& + 2 \sum_{i<j} \text{Im}\left[U_{\alpha i} U_{\beta i}^* U_{\alpha j}^* U_{\beta j}\right] \sin\left(\frac{\Delta m_{ji}^2 L}{2E}\right),
\end{aligned}
\tag{4}
$$

where $\Delta m_{ji}^2 \equiv m_j^2 - m_i^2$ and L is the distance traveled by the neutrino. For antineutrino oscillations, we need to replace U by U^* in Equation (4), which corresponds to changing the sign of the third term. As a consequence, oscillation experiments can reconstruct all rotation angles and the CP phase. They also can measure the squared mass differences among eigenstates. It should be noted that oscillations are sensitive to (squared) mass differences only. Since there are just two independent squared mass differences and three mass eigenstates, the absolute mass neutrino scale or, equivalently, the absolute value of the lightest mass eigenstate cannot be determined by neutrino oscillations through Equation (4). CP violation in the leptonic sector can be established by measuring the difference between $P(\nu_\alpha \to \nu_\beta)$ and $P(\bar{\nu}_\alpha \to \bar{\nu}_\beta)$ if $\alpha \neq \beta$. Since the leading oscillation term, i.e., the second term of Equation (4), depends on a squared sine, determining the signs of Δm_{ij} is also very challenging. The sign of Δm_{12}^2 was determined at the beginning of the century by solar neutrino experiments [5,8] but the sign of $\Delta m_{31}^2 = m_3^2 - m_1^2$ has not been determined yet [9].

Equation (4) cannot be applied to long-baseline experiments without further modifications. Since L implies a long journey of the neutrinos through the Earth's upper crust,

matter effects perturb the oscillation probabilities. Unlike astrophysical neutrinos, where matter perturbations cause a strong change of the probability, the nearly constant, moderate-size matter density represents a small perturbation for accelerator neutrinos that can be accounted for by considering a perturbative expansion of the full oscillation formula and retaining only first-order perturbations in

$$\alpha \equiv \frac{\Delta m_{21}^2}{|\Delta m_{31}^2|} \; . \tag{5}$$

The perturbative expansion of the $\nu_\mu \to \nu_e$ oscillation probability at the second order in α [10,11] is the master formula of long-baseline experiments and deserves careful consideration:

$$
\begin{aligned}
P_{\nu_\mu \to \nu_e} \;\simeq\; & \sin^2 2\theta_{13} \, \sin^2 \theta_{23} \frac{\sin^2[(1-\hat{A})\Delta]}{(1-\hat{A})^2} \\
- \;& \alpha \sin 2\theta_{13} \, \xi \sin \delta \sin(\Delta) \frac{\sin(\hat{A}\Delta)}{\hat{A}} \frac{\sin[(1-\hat{A})\Delta]}{(1-\hat{A})} \\
+ \;& \alpha \sin 2\theta_{13} \, \xi \cos \delta \cos(\Delta) \frac{\sin(\hat{A}\Delta)}{\hat{A}} \frac{\sin[(1-\hat{A})\Delta]}{(1-\hat{A})} \\
+ \;& \alpha^2 \cos^2 \theta_{23} \sin^2 2\theta_{12} \frac{\sin^2(\hat{A}\Delta)}{\hat{A}^2} \\
\equiv \;& O_1 \;+\; O_2(\delta) \;+\; O_3(\delta) \;+\; O_4 \; .
\end{aligned}
\tag{6}
$$

In this formula, $\Delta \equiv \Delta m_{31}^2 L/(4E)$ and the terms contributing to the so-called Jarlskog invariant [5,12] are split into the small parameter $\sin 2\theta_{13}$, the $\mathcal{O}(1)$ term $\xi \equiv \cos \theta_{13} \sin 2\theta_{12} \sin 2\theta_{23}$, and the CP term $\sin \delta$; $\hat{A} \equiv 2\sqrt{2} G_F n_e E / \Delta m_{31}^2$ with G_F representing the Fermi coupling constant and n_e the electron density in matter. The sign of $\hat{A}$ depends on the sign of Δm_{31}^2. A positive (negative) sign of Δm_{31}^2 signifies that the lightest mass eigenstate m_1 is the eigenstate that has the largest mixing with the electron (tau) neutrino [5,6]. It is positive (negative) for the normal (inverted) ordering of neutrino masses. This definition stems from the analogy with quarks. The normal ordering reflects the possible similarity between the mass hierarchy of neutrinos and that of quarks. Evidence for the inverted ordering ($\Delta m_{31}^2 < 0$) would show that the mass hierarchy of the neutrinos follows the opposite quark pattern. In inverted order, the lightest neutrino mass eigenstates are mainly mixed with the tau neutrino, whose charged counterpart (the tau lepton) is the heaviest among charged elementary leptons.

A few considerations are in order:

- The master Formula (6) contains all the parameters of the neutrino Yukawa sector except for the absolute normalization of the masses. This is because the formula depends on Δm_{21}^2 and Δm_{31}^2, but Δm_{32}^2 is just $\Delta m_{31}^2 - \Delta m_{21}^2$. Hence, a full determination of the parameters in Equation (6) fixes only two of the three mass eigenstates. In particular, it does not constrain the lightest mass eigenstate, which remains out of the scope of long-baseline experiments and, in general, neutrino oscillation physics.
- Long-baseline experiments generally aim at $\Delta = \pi/2$ to enhance the oscillation probability. Still, working with a monochromatic beam and only four observables is not enough to disentangle all the parameters. As a consequence, using the whole energy distribution of oscillated neutrinos or, at least, multiple oscillation peaks, provides more redundancy to address the full parameter set.
- The master formula for the corresponding CP state, namely the oscillation probability for $\bar{\nu}_\mu \to \bar{\nu}_e$, is identical to Equation (6) except for a change in the sign of $\mathcal{O}_3$. Long-baseline experiments, therefore, utilize neutrino- and antineutrino-enriched runs to determine $\mathcal{O}_3$ and, consequently, δ.

The relevance of Equation (6) for experimental neutrino physics was established between 2002 and 2012 and brought long-baseline experiments to the forefront of neutrino physics. Long-baseline experiments can easily achieve $\Delta = \pi/2$ (the oscillation peak if we neglect matter effects) because accelerator neutrinos with a mean energy of 1 GeV have $\Delta = \pi/2$ when

$$\frac{\pi}{2} = \Delta = 1.27 \frac{\Delta m_{31}^2(\text{eV}^2) L(\text{km})}{E(\text{GeV})}. \tag{7}$$

Since $\Delta m_{31}^2 \simeq 2.5 \times 10^{-3}$ eV^2 (see Table 1), the oscillation peak at 1 GeV corresponds to a baseline of 495 km and matter effect does not change this finding by more than 20%. The ideal baselines for those facilities are thus well within the range of terrestrial experiments. Thanks to the measurements of Δm_{21}^2 provided by solar [8,13,14] and reactor [15] experiments in the 2000s, we became aware that $\alpha \sim 0.03$. This result boosted proposals for long-baseline beams because the size of the subdominant O_2 and O_3 terms in the master formula are not too small compared with the leading term O_1. Still, the overall size of $P(\nu_\mu \to \nu_e)$ driven by O_1 and the key measurement of θ_{31} only became available in 2012. The value measured by Daya Bay [16], RENO [17], Double Chooz [18], and T2K [19,20] turned out to be very large, just below the previous limits from Chooz [5,21,22]. Indeed, the smallest neutrino mixing angle ($\theta_{13} \simeq 8.6°$) has a size comparable with the Cabibbo angle (13°), i.e., the largest quark mixing angle, and brings the leading term of the master formula to

$$O_1 \simeq 0.04 \frac{\sin^2[(1-\hat{A})\Delta]}{(1-\hat{A})^2}. \tag{8}$$

The discovery of θ_{13} demonstrated that a long-baseline experiment capable of investigating oscillation probabilities at a <1‰ level could reconstruct the neutrino Yukawa sector of the Standard Model, with the exception of determining the size of the lightest mass eigenstate. This realization led to the design and construction of *Superbeams*: neutrino beams generated by megawatt-class proton accelerators, directed towards neutrino detectors of unprecedented mass situated hundreds of kilometers from the sources [23]. These remarkable facilities represent the evolution of long-baseline experiments such as K2K [24], OPERA [2], T2K [25], and NOvA [26], and are the focus of this paper.

Table 1. Current values of the PMNS parameters and neutrino masses as extracted by the NuFit collaboration in 2022. The numbers in the 1st (2nd) column are obtained assuming normal ordering (inverted ordering), i.e., relative to the respective local minimum. It should be noted that $\Delta m_{3\ell}^2 \equiv \Delta m_{31}^2 > 0$ for normal ordering and $\Delta m_{3\ell}^2 \equiv \Delta m_{32}^2 < 0$ for inverted ordering. Additional details are available in [9,21]. Reproduced from [21] under the terms of the Creative Commons CC BY license.

		Normal Ordering (best fit)		Inverted Ordering ($\Delta\chi^2 = 2.3$)	
		bfp $\pm 1\sigma$	3σ range	bfp $\pm 1\sigma$	3σ range
Without SK atmospheric data	$\sin^2\theta_{12}$	$0.303^{+0.012}_{-0.011}$	$0.270 \to 0.341$	$0.303^{+0.012}_{-0.011}$	$0.270 \to 0.341$
	$\theta_{12}/°$	$33.41^{+0.75}_{-0.72}$	$31.31 \to 35.74$	$33.41^{+0.75}_{-0.72}$	$31.31 \to 35.74$
	$\sin^2\theta_{23}$	$0.572^{+0.018}_{-0.023}$	$0.406 \to 0.620$	$0.578^{+0.016}_{-0.021}$	$0.412 \to 0.623$
	$\theta_{23}/°$	$49.1^{+1.0}_{-1.3}$	$39.6 \to 51.9$	$49.5^{+0.9}_{-1.2}$	$39.9 \to 52.1$
	$\sin^2\theta_{13}$	$0.02203^{+0.00056}_{-0.00059}$	$0.02029 \to 0.02391$	$0.02219^{+0.00060}_{-0.00057}$	$0.02047 \to 0.02396$
	$\theta_{13}/°$	$8.54^{+0.11}_{-0.12}$	$8.19 \to 8.89$	$8.57^{+0.12}_{-0.11}$	$8.23 \to 8.90$
	$\delta/°$	197^{+42}_{-25}	$108 \to 404$	286^{+27}_{-32}	$192 \to 360$
	$\dfrac{\Delta m_{21}^2}{10^{-5}\text{ eV}^2}$	$7.41^{+0.21}_{-0.20}$	$6.82 \to 8.03$	$7.41^{+0.21}_{-0.20}$	$6.82 \to 8.03$
	$\dfrac{\Delta m_{3\ell}^2}{10^{-3}\text{ eV}^2}$	$+2.511^{+0.028}_{-0.027}$	$+2.428 \to +2.597$	$-2.498^{+0.032}_{-0.025}$	$-2.581 \to -2.408$

3. The HyperKamiokande Experiment

The T2K experimental facility is anchored by a proton accelerator, the JPARC Proto-Synchrotron, boasting an energy output of 30 GeV and supporting a beamline equipped with three magnetic horns [27,28]. Mesons travel to and decay within a 96-meter-long decay volume. While the facility was initially designed to achieve a nominal power of 750 kW, this benchmark was only recently reached. However, the beamline is structured to accommodate upgrades on a Superbeam scale, with the potential for power enhancements up to a maximum of 1.3 MW. Plans for such an upgrade were in place well before the discovery of θ_{13} [29], but post-2012, it became apparent that an upgraded T2K would be optimally configured to uncover a CP violation in the leptonic sector and precisely measure δ [30]. This ambitious goal necessitates a 1.3 MW beam, contingent upon the availability of a far detector significantly larger than SuperKamiokande (SK). Presently, T2K is nearing completion of its physics program following upgrades to the near detector and the introduction of gadolinium doping in SK, enhancing its neutron tagging efficiency. The cornerstone of the forthcoming HyperKamiokande facility lies in the deployment of a far detector five times the size of SK, leveraging the T2K beam at its maximum 1.3 MW power capacity [31]. Approved in January 2020, the HyperKamiokande project is progressing steadily, with data collection slated to commence in 2027.

HyperKamiokande employs the same detection strategy as T2K. HK will be a water Cherenkov detector with a water mass of 258 kton (fiducial mass: 187 kton). It consists of a cylindrical tank of 68 m diameter and 71 m height. Like SK, the tank volume will be divided into the Inner Detector and the Outer Detector by an inactive cylindrical structure. The structure optically separates the two detector volumes and holds the PMTs looking both inwards to the Inner Detector and outwards to the Outer Detector. The Outer Detector consists of 8 cm PMTs and wavelength shifting plates. It is used to reject cosmic ray muons to constrain the external background.In the Inner Detector, there will be 20,000 50 cm (20 inches) diameter PMTs by Hamamatsu Photonics and approximately 800 multi-PMT modules (mPMTs). The HyperKamiokande PMTs perfect a technique that has been developed in the course of the upgrades from Kamiokande [32] to SuperKamiokande [33] to HyperKamiokande. The HK PMTs have the same size (20″ diameter) as the "Venetian blinds" PMTs used in the Super-Kamiokande detector, but a higher quantum efficiency and different dynode structure. The transit time spread (2.7 ns) is smaller leading to better time resolution at one photo-electron equivalent pulse height. The dark noise is about 4 kHz and each PMT covers about 2000 cm^2. The light yield of 20,000 installed PMTs is about 6 photoelectrons/MeV. Leveraging the studies performed by non-accelerator experiments (JUNO [34] and KM3NeT [35]), HK will also employ about 800 multi-PMTs made of 3″ devices. The 3″ PMTs are not arranged facing parallel directions, but point in slightly different directions. The better granularity and directional sensitivity of these smaller PMTs will thus improve the detector systematics and energy calibration.

The excavation of the HK cavern is unprecedented in neutrino physics. The main cavern consists of a rooftop portion, which is called a "dome section," and a cylindrical "barrel section" under the dome section. The main cavern is approximately 94 m high (the dome section is 21 m high, and the barrel section is 73 m high) with a diameter of 69 m. The total excavation volume of the main cavern is approximately 330,000 m^3 [36]. At the time of writing, most of the access tunnels are available and the excavation of the main cavern is close to completion.

The core upgrade of the T2K beamline in preparation for HK resides in the operating conditions of the PS Main Ring. Since the beam power is inversely proportional to the repetition cycle, and is proportional to the number of protons per pulse, both parameters will be enhanced. At present, the repetition cycle is 2.48 s (2.6×10^{14} protons/cycle) and will be upgraded to 1.16 s (2.3×10^{14} protons/cycle). This implies the replacement of the power supplies for the main magnets and the RF cavities. The HK baseline is very similar to T2K. The detector will be hosted in the Tochibora mine, about 295 km away from the J-PARC proton accelerator research complex in Tokai, Japan. It will lie under the peak of Nijuugo-

yama, with an overburden of 650 m of rock or a 1750 m water equivalent. It will be offset with respect to the beam axis by about 2.5°, as in T2K. The off-axis configuration allows for a narrower energy spread of the incoming neutrinos, whose mean energy will be 0.6 GeV. For such a baseline, matter effects are negligible and $\hat{A} \sim 0.5 \times 10^{-2}$ in Equation (6). As a consequence, the master formula does not depend on the sign of Δm^2_{31}, and CP-violating effects are easier to establish, even when using a beam with a small momentum spread.

The strength of the HK program is twofold. HK offers a clear environment to establish CP violation in the leptonic sector comparing the $\nu_\mu \to \nu_e$ oscillation probability with the corresponding $\bar{\nu}_\mu \to \bar{\nu}_e$ probability measured in $\bar{\nu}_\mu$-enriched runs. In addition, HK showcases impressive physics capabilities with natural neutrino sources given its size and underground location. The observation of atmospheric neutrinos using the same technique employed by SK is particularly rewarding. Since all oscillation parameters are fixed by long-baseline data, HK will employ a large sample of atmospheric ν_μ and ν_e interactions to measure matter effects and establish the sign of Δm^2_{31} using an independent neutrino source. This method partially overcomes the lack of matter effects in beam events and can establish the neutrino ordering using the same technique as SuperKamiokande [37] but with enhanced statistical power.

Figure 1 shows the sensitivity of HK to CP violation as a function of the true value of δ assuming the mass ordering to be measured with HK atmospheric neutrinos or other experiments (JUNO, ORCA, NOνA , and DUNE). The beam from J-PARC is expected to provide 2.7×10^{21} protons-on-target (pots) per year [38]. The sensitivity to δ mainly comes from $\nu_\mu \to \nu_e$'s appearance, while the sensitivity to $\sin^2 \theta_{23}$ and Δm^2_{31} is mostly due to disappearance data ($\nu_\mu \to \nu_\mu$). Since the flux and cross-section of antineutrinos at 0.6 GeV is about three times smaller than neutrinos, the HK collaboration is planning to increase the duration of $\bar{\nu}_\mu$-enriched runs at a ratio of 3:1 compared with the ν_μ-enriched runs. HK is very sensitive to CP violation and can get higher than eight σ significance for excluding CP conservation, assuming the mass ordering is known. After 10 years of data collection, CP conservation will be excluded for 61% of true values of δ assuming normal ordering.
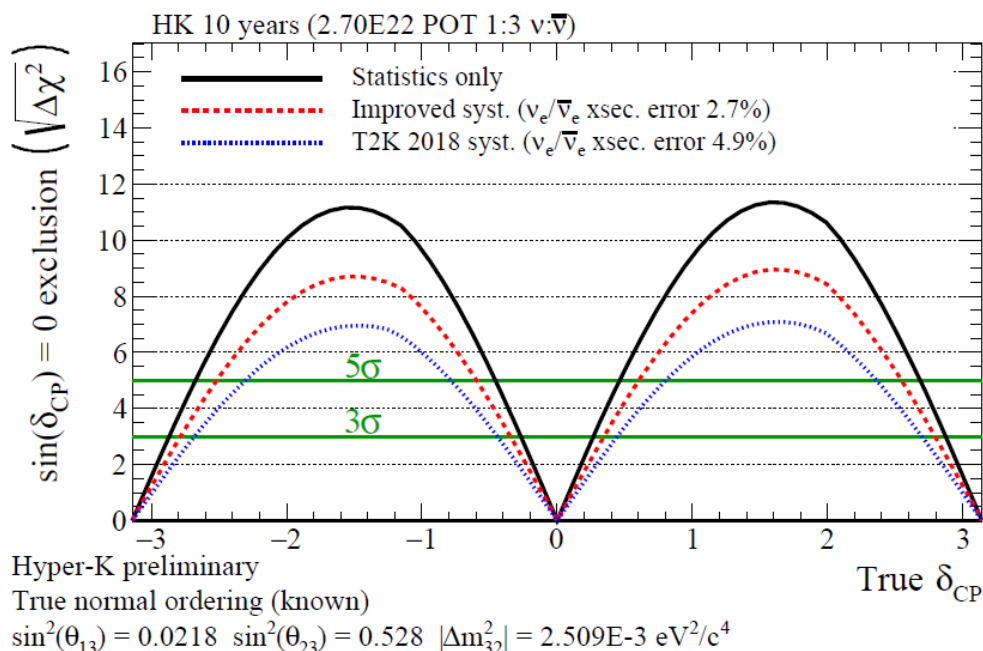

Figure 1. HyperKamiokande's sensitivity to CP violation projected over a 10-year period, assuming the normal mass ordering. Reproduced from [38] under the CC BY 4.0 license.

HK is not expected to improve oscillation parameters such as θ_{12} and Δm^2_{21} compared to dedicated reactor experiments like JUNO [39]. This is because the dependence of the master formula on these parameters is weak, and the observation of oscillations at the 'solar

peak' by reactor or solar neutrino experiments is more effective. This oscillation maximum corresponds to

$$\frac{\pi}{2} = \Delta_{sol} \equiv \frac{\Delta m_{12}^2}{4E} = 1.27 \frac{\Delta m_{21}^2 (\text{eV}^2) L(\text{km})}{E(\text{GeV})} \tag{9}$$

and long-baseline accelerator neutrino experiments usually operate far from this peak. In the master formula, the large distance from the solar peak of accelerator neutrinos corresponds to the α suppressions of the terms representing three-family interference (O_2 and O_3), as well as the α^2 term O_4, which is due to the oscillations driven by Δm_{21}^2. Conversely, HK and DUNE will play a key role in understanding whether the mixing induced by θ_{23} is maximal ($\theta_{23} = 45°$) or deviates from maximality. The determination of the *octant* of θ_{23}, which is of relevance for flavor models, can be established by HK. The wrong octant can be excluded at 3σ for true $\sin^2 \theta_{23} < 0.47$ and true $\sin^2 \theta_{23} > 0.55$.

The physics capabilities of HK hinge on a comprehensive systematic reduction program, as both HK and DUNE stand to gain from the unparalleled statistics generated by the beam intensity and detector size. Systematic uncertainties are primarily tackled by the near detector, which tightly constrains the flux prior to oscillations. This detector plays a pivotal role in mitigating other sources of systematic uncertainty, such as cross-section uncertainties and detector inefficiencies. Additionally, the reduction program incorporates ancillary measurements, such as hadroproduction experiments utilizing an HK replica target, or novel assessments of neutrino cross-sections derived from specialized experiments [40]. This underscores why the near detector complexes of HK and DUNE are the most advanced facilities proposed to date.

In addition to the T2K near detector upgrade [41], the HK collaboration is planning an intermediate water Cherenkov detector [31]. The detector utilizes an innovative design pioneered by the PRISM collaboration [42] for HK and also adopted by DUNE. The intermediate water Cherenkov detector (IWCD) of HK will consist of a tall vertical shaft outfitted with multiple PMTs, situated roughly 1 km from the beam source. The IWCD is movable along the shaft in the vertical direction, allowing for off-axis angles ranging from one to four degrees. This flexibility enables the monitoring of the beam at various energies, including the off-axis angle relevant to HK, facilitating a data-driven modeling approach for extrapolating the flux from the near to the far detector. The IWCD will also detect events using the same water Cherenkov technology as the far detector, as the event rate at 1 km is manageable and the overlap of Cherenkov rings from different events is negligible. Employing a water Cherenkov detector at the near location (250 m) is not feasible due to the unprecedented beam intensity. Instead, the near detector of T2K/HK relies on alternative techniques, which may introduce efficiency biases in the extrapolation from the near to the far detector.

4. The DUNE Experiment

The design approach of DUNE differs significantly from that of HK [43]. While water Cherenkov detectors provide scalability advantages due to the low cost of the target material (water), they come with limitations in resolution. Reconstruction of neutrino interactions is hindered by final state particles below the Cherenkov threshold and by events with large multiplicities, leading to overlapping Cherenkov rings. In contrast, DUNE utilizes detectors much smaller than HK but focuses on achieving precise neutrino reconstruction through the use of liquid argon time projection chambers (LArTPC).

The DUNE project encompasses two primary facilities aimed at supporting the US particle and astroparticle physics program in the coming years. The first facility is a new Superbeam that utilizes the same proton accelerator as NOvA but with enhanced performance [44]. Neutrinos are produced after the protons hit a solid target and produce mesons, which are subsequently focused by three magnetic horns into a 194 m long helium-filled decay pipe where they decay into muons and neutrinos. Protons (120 GeV) are provided by the Fermilab Main Injector, which is expected to deliver 1.2 MW for the DUNE/LBNF program, with the PIP-II upgrade, corresponding to 1.1×10^{21} protons on

target per year. This setup will serve Phase I of DUNE, where a wide-band neutrino beam with a mean energy of approximately 2.5 GeV will reach two LArTPCs located 1300 km from the source. Each TPC will contain 17 kton of liquid argon, corresponding to a fiducial mass of about 10 kton per TPC. DUNE will undergo further upgrades in Phase II, during which the beam intensity will progressively increase to over 2.1 MW, and the beam will serve up to four LArTPCs, resulting in a total fiducial mass of about 40 kton.

The second facility is a large underground laboratory currently under construction in Lead, South Dakota. Known as the Sanford Underground Research Facility (SURF), it will host the DUNE TPCs and is situated within the former Homestake Gold Mine. SURF already serves as the host laboratory for dark matter experiments (such as LZ [45]) and neutrinoless double beta decay experiments (such as the Majorana Demonstrator). Excavation of the underground halls and ancillary facilities for DUNE was completed in February 2024, and preparations are underway for the installation of the DUNE cryostats.

A notable characteristic of the DUNE neutrino beam (LBNF) is the momentum range of the produced neutrinos. Unlike HK, DUNE is situated along the axis of a wide-band beam. Consequently, DUNE captures oscillations from the first (2.5 GeV) to the second (0.6 GeV) oscillation peak. Observing the entire sinusoidal pattern of $\nu_\mu \to \nu_e$ oscillations in a single detector enhances the potential to disentangle the effects of the $O_{1,2,3}$ operators in the master formula. This capability is exclusive to high-resolution detectors like the LArTPCs and is pivotal in unraveling the correlation among the oscillation parameters. Specifically, DUNE can concurrently measure the magnitude of δ, the sign of Δm_{31}^2 (mass ordering), and the octant of θ_{23} without the need for external information.

The first DUNE LArTPC [46] builds upon the knowledge acquired from ICARUS [47] and MicroBOONE [48], with an emphasis on scalability given the substantially larger TPC mass compared to ICARUS (600 t). The TPC drift length is 3.5 m and the cathode is operated at -180 kV. To accommodate the relatively short drift length, each TPC features two cathodes and three anodes, as illustrated in Figure 2. The anode wires are arranged within modules called Anode Plane Assemblies (APAs), measuring 6×2.3 m^2. These APAs are assembled on-site. They both simplify construction and remove the necessity for wires of much greater length compared to those used in ICARUS. The TPC components are thus designed to be modular, allowing for on-site assembly in the underground laboratory, and the cryogenic system has been significantly streamlined. In 2016, ProtoDUNE-SP demonstrated the feasibility of achieving an electron lifetime comparable to that of ICARUS using a cryostat based on cost-effective technology originally developed for industrial applications [49]. A "membrane cryostat" consists of a corrugated membrane that contains both liquid and gaseous argon, along with a passive insulation system to minimize heat leakage. The structure also includes a reinforced concrete framework to support the pressure exerted by the contents. Additionally, a secondary barrier system integrated into the insulation protects against potential spills of liquid argon, while a vapor barrier applied over the concrete safeguards the insulation from moisture. This system, traditionally employed in the transportation of liquefied natural gases, has been adapted and refined for use with high-purity argon during the research and development phase of DUNE. The use of membrane cryostats remarkably simplified the design of DUNE and this technology will be employed for all DUNE TPCs.

Unlike ICARUS, the charge readout electronics are positioned within the cold volume to minimize noise. This approach enhances noise reduction and decreases the requirement for cryostat penetrations to read the signals from the anodes. Similar to any LArTPC, DUNE also captures the 128 nm scintillation light generated in liquid argon by charged particles. However, significant changes have been made to the light detection system compared to previous detectors. The DUNE system employs a compact device (X-ARAPUCA [50,51]) that shifts the photon wavelength toward values that are more amenable to detection by SiPMs and traps those photons inside a finite volume, whose walls are covered by SiPMs. The compact nature of the system enables it to be positioned inside the APA, right before the (semi-transparent) wires of the TPC.
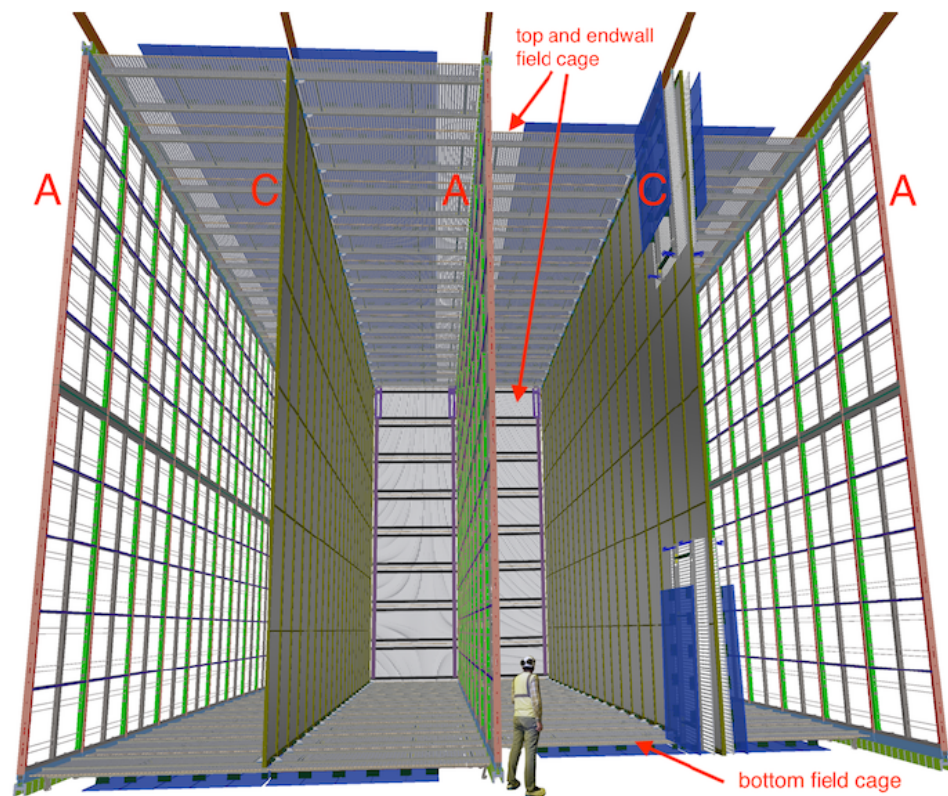
Figure 2. The DUNE Horizontal Drift liquid argon TPC, showing the alternating 58.2 m long (into the page), 12.0 m high anode (A) and cathode (C) planes, as well as the field cage (FC) that surrounds the drift regions between the anode and cathode planes. For the sake of illustration, on the right-hand cathode plane, the foremost portion of the FC is shown in its undeployed (folded) state. Reproduced from [46] under the CC BY 4.0 license.

The second DUNE TPC [52], known as the "Vertical Drift," capitalizes on the advancements in LArTPC technology made over the past decade. Building on the exceptional performance of the membrane cryostats and the purification system demonstrated in ProtoDUNE-SP, the Vertical Drift TPC features a 6.5 m drift length, with the electric field generated by a cathode positioned in the center of the TPC at -300 kV. Consequently, the ionization electrons drift vertically towards two anodes situated at the bottom and top of the TPC. Additionally, the anode wires are replaced with strips on PCBs, presenting an innovative design that further streamlines detector construction and reduces costs compared to the APA solution used in the first TPC ("Horizontal Drift"). While the photon detection system still relies on the X-ARAPUCA technology, these devices cannot be installed in the anode due to the opacity of the charge readout strips to light. Instead, in the DUNE Vertical Drift, photon detectors are positioned in the lateral walls of the cryostat just outside the (semi-transparent) field cage and in the cathode. However, since the cathode operates at a -300 kV voltage reference, these devices cannot be read and powered by standard copper cables due to discharge risks. Consequently, the signal is converted into light pulses using commercial optocouplers operated at the temperature of liquid argon (87 K) and transmitted via optical fibers (Signal-over-Fiber). The same technique is used with high-power lasers (Power-over-Fiber) to provide power to the cold electronics and SiPMs used for photon detection.

The DUNE near detector serves multiple purposes, including monitoring the neutrino flux and flavor at the source, obtaining detailed information on beam composition, detecting spectrum biases in near-to-far extrapolation, and mitigating cross-section uncertainties [53]. A crucial component of the DUNE ND is an LArTPC built using ArgonCube technology, known as ND-LAr. This detector shares the same target nucleus and fundamental detection

principles as the far detector but is specifically designed to handle the high event rate near the source. However, ND-LAr begins to lose muon acceptance above 0.7 GeV/c due to lack of containment, necessitating the use of a muon spectrometer as a complement. Both detectors can be horizontally moved perpendicular to the beam axis, employing the same PRISM technique as the HK intermediate Water Cherenkov detector.

The SAND [53,54] detector, located on the beam axis, serves as the final component of the DUNE near detector suite. This magnetized beam monitor is crucial for monitoring the neutrino flux heading to the far detector from an on-axis position, where it exhibits higher sensitivity to variations in the neutrino beam. SAND utilizes the KLOE magnet and calorimeter, originally employed for kaon physics studies at the DAΦNE collider since the 1990s [55], now repurposed for DUNE by the Italian Institute for Nuclear Research (INFN). SAND comprises an inner tracker surrounded by the KLOE electromagnetic calorimeter within a large solenoidal magnet. The tracker is composed of straw-tubes, while the magnet features a superconducting coil generating a 0.6 T magnetic field. The calorimeter is a high-resolution, high-granularity lead-scintillator sampling e.m. calorimeter.

DUNE will achieve unparalleled sensitivity in determining mass ordering due to its long baseline and utilization of a wide-band beam. It is projected to determine the sign of Δm^2_{31} within approximately 2 years of Phase I of data collection, scheduled to commence in 2030. The ultimate sensitivity regarding the CP phase and the θ_{23} octant is anticipated during Phase II. Figures 3 and 4 show, in particular, the precision that can be achieved in the measurement of δ and θ_{23} after 10 years of data taking.

DUNE's underground location at SURF, with an overburden of about 4300 m water equivalent (1490 m of rock), enables a diverse physics program involving natural sources. It thus complements the HyperKamiokande program. Thanks to the larger mass, HK provides unique sensitivity to proton decay in the $p \to e^+ \pi^0$ mode while DUNE is competitive in the $p \to K^+ \bar{\nu}$ mode because the kaon is below the Cherenkov threshold. Similarly, HK offers unparalleled statistics in the event of a galactic supernova explosion, while DUNE can exploit the larger ν_e CC cross-section in argon compared with the $\nu - e$ elastic scattering typically used in water Cherenkov detectors.
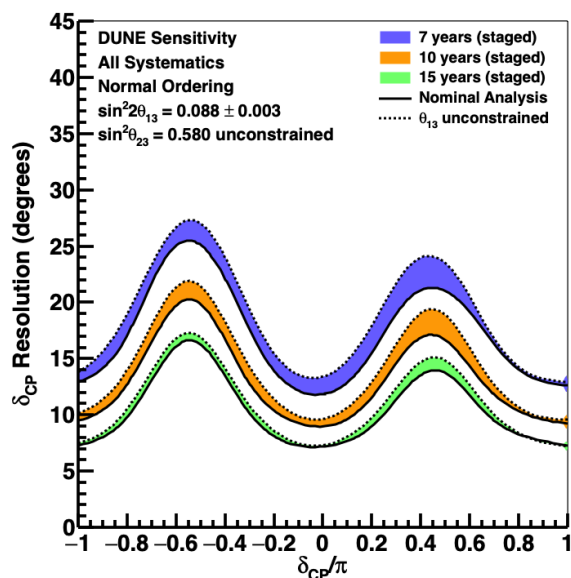

Figure 3. Resolution in degrees for the DUNE measurement of δ, as a function of the true value of δ, for seven (blue), ten (orange), and fifteen (green) years of exposure. The width of the band shows the impact of applying an external constraint on θ_{13}. Reproduced from [56] under the terms of the Creative Commons CC BY license.
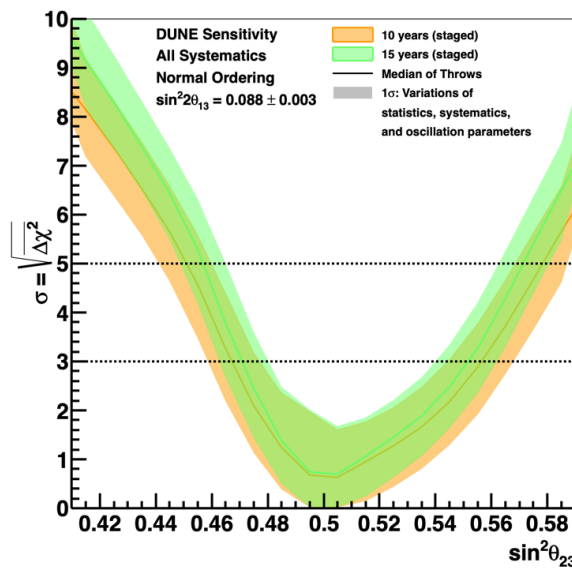
Figure 4. Sensitivity to the determination of the θ_{23} octant as a function of the true value of $\sin^2 \theta_{23}$, for ten (orange) and fifteen (green) years of exposure, for normal mass ordering. Reproduced from [56] under the terms of the Creative Commons CC BY license.

5. New Facilities

DUNE and HyperKamiokande will capitalize on the physics potential of Superbeams over the next twenty years, but the long-baseline concept has not yet exhausted its opportunities. Novel facilities are currently under study, and in the following, we focus on two concepts. The former does not require any technological advances in accelerator neutrino beams; it is based on the exploitation of the second oscillation maximum to achieve unprecedented precision in the oscillation parameters. The latter would represent a breakthrough in experimental physics as it is based on the production, storage, and decay of muons rather than pions.

5.1. The Second Oscillation Maximum

DUNE has the capability to access both the first and second oscillation maximum, where neutrino interactions are predominantly characterized by quasi-elastic scattering. This region is particularly advantageous for Cherenkov detectors, as events typically manifest as single rings corresponding to the outgoing lepton. The neutrino energy in, e.g., $\nu + n \rightarrow \mu^- + p$, can be safely reconstructed from the lepton energy:

$$E_\nu = \frac{m_p^2 - (m_n - E_b)^2 - m_\mu^2 + 2(m_n - E_b)E_\mu}{2(m_n - E_b - E_\mu + p_\mu \cos \theta_\mu)} \tag{10}$$

where E_b is the neutron binding energy inside the nucleus and θ_μ is the muon direction.

To enhance the physics capabilities of long-baseline experiments, researchers have explored the potential of utilizing a water Cherenkov detector with a significantly larger mass than DUNE to better exploit the information available at the second oscillation maximum (see Figure 5). This opportunity has been under investigation since 2004 [57] and has led to several proposals, including an upgrade of the HK facility with a second detector located in Korea [58]. The Korean Neutrino Observatory (KNO) comprises a detector with a size comparable to HK located in Mt. Biseul (Korea), 1088 km away from JPARC. Due to the longer distance, the statistics accumulated by the Korean detector would be 10 times less than HK but oscillations would be driven by matter effects due to the larger $\hat{A}$ term in the master formula. KNO combined with HK can thus disentangle the effects of mass ordering and CP violation, gaining both an excellent sensitivity to the sign of Δm_{23}^2 and an improved precision in δ.
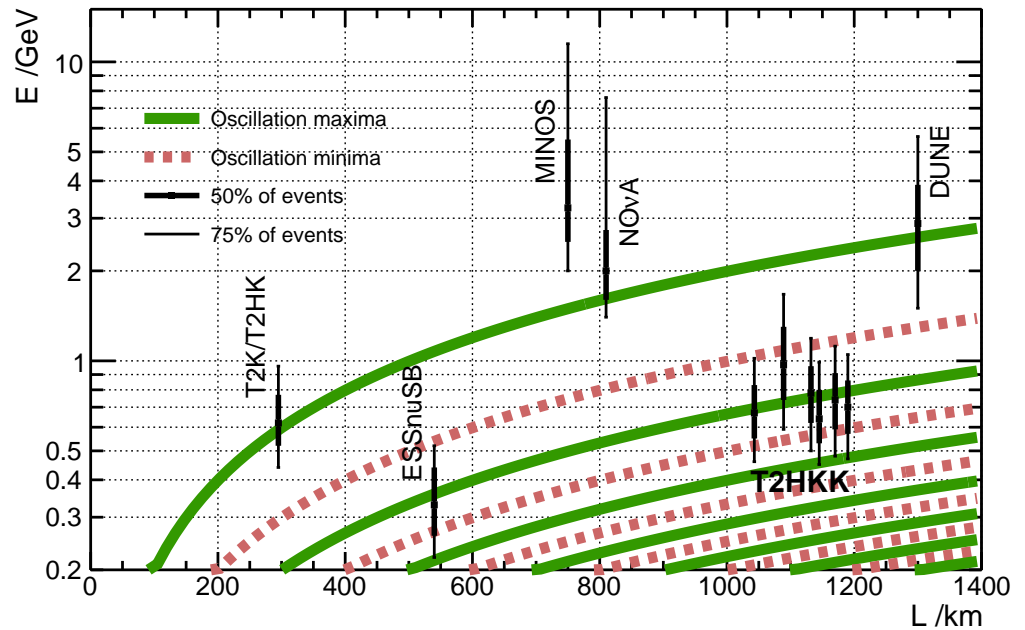
Figure 5. Comparison of baseline and energy regime of various recent and proposed long-baseline experiments. Reproduced from [58] under the terms of the Creative Commons CC BY license.

The use of the second oscillation maximum has also presented an intriguing opportunity for a long-baseline facility in Europe. Europe boasts a powerful proton accelerator that serves the European Spallation Source (ESS), which is set to commence operation very soon. The ESS LINAC reaches an unprecedented 5 MW power, serving a community in pure and applied physics by producing an intense neutron source. The ESSnuSB collaboration has proposed an upgrade of this facility, aiming to reduce the proton pulse length from 2.86 ms to 1.3 μs using a proton accumulator. This shortened pulse duration would enable the use of standard magnetic horns for beam focusing, effectively transforming the ESS into a Superbeam facility [59,60]. Operating at the second oscillation maximum, the facility aims to achieve superior sensitivity in detecting the CP violation phase δ. The rationale is given, again, by Equation (6). Since the energy of the upgraded ESS LINAC (2.5 GeV proton kinetic energy) is much smaller than the JPARC Proto-Synchrotron, the mean neutrino energy is 0.35 GeV and the second maximum is located at $L \simeq 360$ km. Given the small size of matter effects, we can rewrite the master formula in a vacuum and determine the size of CP-violating effects. If we define the CP asymmetry as

$$\mathcal{A} = P(\nu_\mu \to \nu_e) - P(\bar{\nu}_\mu \to \bar{\nu}_e) \tag{11}$$

we have, in natural units,

$$\mathcal{A} = -16J \sin\frac{\Delta m_{31}^2 L}{4E} \sin\frac{\Delta m_{32}^2 L}{4E} \sin\frac{\Delta m_{21}^2 L}{4E} \tag{12}$$

where $J \sim \sin\theta_{13} \sin\delta$ is the Jarlskog invariant. Following [60], we can compute the asymmetry ratio between the second and first oscillation maxima, corresponding to $\Delta = 3\pi/2$ and $\Delta = \pi/2$, respectively,

$$\frac{\mathcal{A}(2^o \text{ max})}{\mathcal{A}(1^o \text{ max})} \simeq 2.7 \ . \tag{13}$$

At the second maximum, CP-violating effects are enhanced by nearly a factor of three, contingent upon the ESS LINAC's ability to offset the reduction in statistics resulting from the relatively long baseline and low neutrino energy. The ESSnuSB project proposes a

HK-like water Cherenkov detector situated in the Zinkgruvan mine in Sweden, 360 km from the neutrino beam source. This facility can reach precision in δ ranging from 7.5 to 4.5 degrees and search for new physics in the lepton sector [61].

The ESS LINAC holds significant potential for contributing to neutrino physics, even in the construction stages of the ESSnuSB project. This potential is currently being explored within the framework of the ESSnuSB+ design study. Specifically, utilizing less than 10% of the current LINAC's power, without requiring any upgrades, can support a monitored neutrino beam based on the ENUBET concept [62,63]. This beam would enable the measurement of neutrino cross-sections at the percent level below 1 GeV. Additionally, operating the ESS LINAC at 1/4 of its maximum power, combined with the proton accumulator, could supply a potential muon storage ring for neutrino physics utilizing the NuSTORM concept, as elaborated below.

5.2. Beyond Superbeams

The primary constraint of current long-baseline experiments lies in their reliance on sources such as Superbeams, which exclusively generate ν_μ and $\overline{\nu}_\mu$ neutrinos. Consequently, the only observables that can be exploited are the ones of Equation (1). This feature limits the possibility of performing unitary tests of the PMNS matrix and searching for physics beyond the Standard Model. A source employing muons instead of pions to produce neutrinos would allow for ν_e-based long-baseline experiments exploring the T conjugate of $\nu_\mu \rightarrow \nu_e$, that is, $\nu_e \rightarrow \nu_\mu$, and, even more, the $\nu_e \rightarrow \nu_\tau$ oscillation probability that is key to probe deviations from unitarity.

The concept of generating muons through pion decays and storing them in a ring has been under investigation for decades, primarily in anticipation of a potential muon collider [64,65]. However, the technological hurdles associated with a muon collider are significant. One major challenge involves ensuring that the emittance of the produced muons is suitable for collider applications. Muon cooling thus presents a substantial obstacle that must be overcome before such a facility can be realized. If our objective is to store muons or antimuons and allow them to decay, thereby generating a focused flux of neutrinos in the straight section of the decay ring, many of these constraints can be significantly relaxed.

This idea forms the foundation of the Neutrino Factory concept [66–68], where an unparalleled flux of ν_e and $\overline{\nu}_e$ could be generated both below and above the kinematic threshold for the tau lepton production to study $\nu_e \rightarrow \nu_\mu$ and $\nu_e \rightarrow \nu_\tau$ oscillations. Many of the technology challenges for a Neutrino Factory were conceptually addressed prior to the discovery of θ_{13}. After 2012, research and development in this area somewhat slowed down to prioritize Superbeams, as these facilities are sufficient to investigate the lepton Yukawa sector of the Standard Model, as demonstrated earlier. Nevertheless, a Neutrino Factory remains the sole option to attain a level of understanding of the PMNS matrix comparable to that of the CKM matrix. In the course of these advancements, the MICE experiment has validated the fundamental principles of muon cooling [69], and various laboratories worldwide are exploring the development of a muon collider demonstrator to achieve the anticipated level of cooling. An important intermediate step is the deployment of the NuSTORM facility, which is aimed at muon storage without cooling [70]. By utilizing the straight section of the muon storage ring in conjunction with a short-baseline neutrino experiment, NuSTORM aims to yield substantial statistics of electron neutrinos within the energy range relevant to DUNE and HK. NuSTORM thus advances the monitored neutrino beams and measures electron neutrino cross-sections with sub-percent precision. The NuSTORM design has primarily centered around utilizing the Fermilab Main Ring and the CERN SPS proton accelerator. However, more recent investigations have extended to include the CERN PS for the muon collider demonstrator and within the framework of ESSnuSB+ to examine electron neutrino cross-sections below 1 GeV.

6. Conclusions

Long-baseline neutrino experiments have the potential to probe the entire lepton Yukawa sector of the Standard Model, with the exception of determining the size of the lightest mass eigenstate. This opportunity arises from the large size of the θ_{13} angle, which was first determined in 2012. In this paper, we have outlined how forthcoming long-baseline experiments will capitalize on this opportunity. The primary projects currently in progress are DUNE and HyperKamiokande. These endeavors aim to address the outstanding aspects of the Yukawa sector, including mass ordering, CP phase, and the θ_{23} octant, beginning in 2027. By approximately 2035, it is anticipated that we will have gained a comprehensive understanding of the PMNS structure and mass hierarchy, alongside two expansive underground observatories facilitating a diverse astroparticle physics program. In addition to DUNE and HK, the neutrino physics community is exploring the potential of leveraging the second oscillation maximum and transitioning beyond Superbeam technology towards the realization of a muon-based Neutrino Factory.

Conflicts of Interest: The author declares no conflicts of interest.

References

1. Kopp, S. Accelerator neutrino beams. *Phys. Rep.* **2007**, *439*, 101–159. [CrossRef]
2. Agafonova, N. et al. [OPERA Collaboration] Final Results of the OPERA Experiment on ν_τ Appearance in the CNGS Neutrino Beam. *Phys. Rev. Lett.* **2018**, *120*, 211801; Erratum in *Phys. Rev. Lett.* **2018**, *121*, 139901. [CrossRef]
3. Abbasi, R. et al. [IceCube Collaboration] Measurement of atmospheric neutrino mixing with improved IceCube DeepCore calibration and data processing. *Phys. Rev. D* **2023**, *108*, 012014, [CrossRef]
4. Schumann, J. Neutrino Oscillation Measurements with KM3NeT/ORCA. *Phys. Sci. Forum* **2023**, *8*, 35. [CrossRef]
5. Workman, R.L. et al. [PDG Collaboration] Review of Particle Physics. *Prog. Theor. Exp. Phys.* **2022**, *2022*, 083C01. [CrossRef]
6. Giunti, C.; Kim, C.W. *Fundamentals of Neutrino Physics and Astrophysics*; Oxford University Press: Oxford, UK, 2007.
7. Fukuda, Y. et al. [SuperKamiokande Collaboration] Evidence for oscillation of atmospheric neutrinos. *Phys. Rev. Lett.* **1998**, *81*, 1562–1567. [CrossRef]
8. Ahmad, Q.R. et al. [SNO Collaboration] Direct evidence for neutrino flavor transformation from neutral current interactions in the Sudbury Neutrino Observatory. *Phys. Rev. Lett.* **2002**, *89*, 011301. [CrossRef]
9. Esteban, I. et al. [NuFIT Collaboration] NuFIT 5.2 (2022), 2022. Available online: www.nu-fit.org (accessed on 13 May 2024).
10. Cervera, A.; Donini, A.; Gavela, M.B.; Gomez Cadenas, J.J.; Hernandez, P.; Mena, O.; Rigolin, S. Golden measurements at a neutrino factory. *Nucl. Phys. B* **2000**, *579*, 17–55; Erratum in *Nucl. Phys. B* **2001**, *593*, 731–73. [CrossRef]
11. Freund, M. Analytic approximations for three neutrino oscillation parameters and probabilities in matter. *Phys. Rev. D* **2001**, *64*, 053003. [CrossRef]
12. Jarlskog, C. Commutator of the Quark Mass Matrices in the Standard Electroweak Model and a Measure of Maximal CP Nonconservation. *Phys. Rev. Lett.* **1985**, *55*, 1039. [CrossRef]
13. Aharmim, B. et al. [SNO Collaboration] Combined Analysis of all Three Phases of Solar Neutrino Data from the Sudbury Neutrino Observatory. *Phys. Rev. C* **2013**, *88*, 025501. [CrossRef]
14. Arpesella, C. et al. [Borexino Collaboration] Direct Measurement of the Be-7 Solar Neutrino Flux with 192 Days of Borexino Data. *Phys. Rev. Lett.* **2008**, *101*, 091302. [CrossRef]
15. Abe, S. et al. [KamLAND Collaboration] Precision Measurement of Neutrino Oscillation Parameters with KamLAND. *Phys. Rev. Lett.* **2008**, *100*, 221803. [CrossRef]
16. An, F.P. et al. [DayaBay Collaboration] A side-by-side comparison of Daya Bay antineutrino detectors. *Nucl. Instrum. Meth. A* **2012**, *685*, 78–97. [CrossRef]
17. Ahn, J.K. et al. [RENO Collaboration] Observation of Reactor Electron Antineutrino Disappearance in the RENO Experiment. *Phys. Rev. Lett.* **2012**, *108*, 191802. [CrossRef]
18. Abe, Y. et al. [Double Chooz Collaboration] Reactor electron antineutrino disappearance in the Double Chooz experiment. *Phys. Rev. D* **2012**, *86*, 052008. [CrossRef]
19. Abe, K. et al. [T2K Collaboration] Indication of Electron Neutrino Appearance from an Accelerator-produced Off-axis Muon Neutrino Beam. *Phys. Rev. Lett.* **2011**, *107*, 041801, [CrossRef]
20. Abe, K. et al. [T2K Collaboration] Evidence of Electron Neutrino Appearance in a Muon Neutrino Beam. *Phys. Rev. D* **2013**, *88*, 032002. [CrossRef]

21. Esteban, I.; Gonzalez-Garcia, M.C.; Maltoni, M.; Schwetz, T.; Zhou, A. The fate of hints: Updated global analysis of three-flavor neutrino oscillations. *J. High Energy Phys.* **2020**, *9*, 178. [CrossRef]
22. Apollonio, M. et al. [Chooz Collaboration] Search for neutrino oscillations on a long baseline at the CHOOZ nuclear power station. *Eur. Phys. J. C* **2003**, *27*, 331–374. [CrossRef]
23. Bishay, M. Overview of High Power Neutrino Beams. Talk Presented at the International Workshop on Next Generation Nucleon Decay and Neutrino Detectors (NNN19). 2019. Available online: https://indico.cern.ch/event/835190/ (accessed on 13 May 2024).
24. Ahn, M.H. et al. [K2K Collaboration] Measurement of Neutrino Oscillation by the K2K Experiment. *Phys. Rev. D* **2006**, *74*, 072003. [CrossRef]
25. Abe, K. et al. [T2K Collaboration] Observation of Electron Neutrino Appearance in a Muon Neutrino Beam. *Phys. Rev. Lett.* **2014**, *112*, 061802. [CrossRef] [PubMed]
26. Acero, M.A. et al. [NOvA Collaboration] First Measurement of Neutrino Oscillation Parameters using Neutrinos and Antineutrinos by NOvA. *Phys. Rev. Lett.* **2019**, *123*, 151803. [CrossRef] [PubMed]
27. Abe, K. et al. [T2K Collaboration] The T2K Experiment. *Nucl. Instrum. Meth. A* **2011**, *659*, 106–135. [CrossRef]
28. Abe, K. et al. [T2K Collaboration] T2K neutrino flux prediction. *Phys. Rev. D* **2013**, *87*, 012001; Addendum in *Phys. Rev. D* **2013**, *87*, 019902. [CrossRef]
29. Nakamura, K. Hyper-Kamiokande: A next generation water Cherenkov detector for a nucleon decay experiment. In Proceedings of the Workshop on Neutrino Oscillations and Their Origin, Tokyo, Japan, 6–8 December 2000; pp. 359–363.
30. Abe, K. et al. [HyperKamiokande Collaboration] A Long Baseline Neutrino Oscillation Experiment Using J-PARC Neutrino Beam and Hyper-Kamiokande. *arXiv* **2014**, arXiv:1412.4673. arXiv:physics.ins-det/1412.4673.
31. Abe, K. et al. [HyperKamiokande Collaboration] Hyper-Kamiokande Design Report. *arXiv* **2018**, arXiv:1805.04163. arXiv:physics.ins-det/1805.04163.
32. Hirata, K.S. et al. [Kamiokande Collaboration] Observation of a small atmospheric muon-neutrino / electron-neutrino ratio in Kamiokande. *Phys. Lett. B* **1992**, *280*, 146–152. [CrossRef]
33. Fukuda, Y. et al. [SuperKamiokande Collaboration] The Super-Kamiokande detector. *Nucl. Instrum. Meth. A* **2003**, *501*, 418–462. [CrossRef]
34. An, F. et al. [JUNO Collaboration] Neutrino Physics with JUNO. *J. Phys. G* **2016**, *43*, 030401. [CrossRef]
35. Adrian-Martinez, S. et al. [KM3Net Collaboration] Letter of intent for KM3NeT 2.0. *J. Phys. G* **2016**, *43*, 084001. [CrossRef]
36. Abe, K.; Tanaka, H.K. Hyper-Kamiokande construction status and prospects. *Front. Phys.* **2024**, *12*, 1378254. [CrossRef]
37. Jiang, M. et al. [SuperKamiokande Collaboration] Atmospheric Neutrino Oscillation Analysis with Improved Event Reconstruction in Super-Kamiokande IV. *Prog. Theor. Exp. Phys.* **2019**, *2019*, 053F01. [CrossRef]
38. Xie, Z. Oscillation physics with Hyper-Kamiokande. In Proceedings of the Neutrino Oscillation Workshop, Ostuni, Italy, 4–11 September 2022. [CrossRef]
39. Abusleme, A. et al. [JUNO Collaboration] Sub-percent precision measurement of neutrino oscillation parameters with JUNO. *Chin. Phys. C* **2022**, *46*, 123001. [CrossRef]
40. Branca, A.; Brunetti, G.; Longhin, A.; Martini, M.; Pupilli, F.; Terranova, F. A New Generation of Neutrino Cross Section Experiments: Challenges and Opportunities. *Symmetry* **2021**, *13*, 1625. [CrossRef]
41. Abe, K. et al. [T2K Collaboration] T2K ND280 Upgrade—Technical Design Report. *arXiv* **2019**, arXiv:1901.03750. arXiv:physics.ins-det/1901.03750.
42. Bhadra, S. et al. [NuPrism Collaboration] Letter of Intent to Construct a nuPRISM Detector in the J-PARC Neutrino Beamline. *arXiv* **2014**, arXiv:1412.3086. arXiv:physics.ins-det/1412.3086.
43. Abi, B. et al. [DUNE Collaboration] Deep Underground Neutrino Experiment (DUNE), Far Detector Technical Design Report, Volume I Introduction to DUNE. *J. Instrum.* **2020**, *15*, T08008. [CrossRef]
44. Strait, J. et al. [DUNE Collaboration] Long-Baseline Neutrino Facility (LBNF) and Deep Underground Neutrino Experiment (DUNE): Conceptual Design Report, Volume 3: Long-Baseline Neutrino Facility for DUNE June 24, 2015. *arXiv* **2016**, arXiv:1601.05823 arXiv:physics.ins-det/1601.05823.
45. Aalbers, J. et al. [LZ Collaboration] First Dark Matter Search Results from the LUX-ZEPLIN (LZ) Experiment. *Phys. Rev. Lett.* **2023**, *131*, 041002. [CrossRef]
46. Abi, B. et al. [DUNE Collaboration] Deep Underground Neutrino Experiment (DUNE), Far Detector Technical Design Report, Volume IV: Far Detector Single-phase Technology. *J. Instrum.* **2020**, *15*, T08010. [CrossRef]
47. Amerio, S. et al. [ICARUS Collaboration] Design, construction and tests of the ICARUS T600 detector. *Nucl. Instrum. Meth. A* **2004**, *527*, 329–410. [CrossRef]
48. Acciarri, R. et al. [MicroBooNE Collaboration] Design and Construction of the MicroBooNE Detector. *J. Instrum.* **2017**, *12*, P02017. [CrossRef]
49. Abud, A.A. et al. [DUNE Collaboration] Design, construction and operation of the ProtoDUNE-SP Liquid Argon TPC. *J. Instrum.* **2022**, *17*, P01005. [CrossRef]
50. Machado, A.; Segreto, E. ARAPUCA a new device for liquid argon scintillation light detection. *J. Instrum.* **2016**, *11*, C02004. [CrossRef]

51. Machado, A.; Segreto, E.; Warner, D.; Fauth, A.; Gelli, B.; Máximo, R.; Pissolatti, A.; Paulucci, L.; Marinho, F. The X-ARAPUCA: An improvement of the ARAPUCA device. *J. Instrum.* **2018**, *13*, C04026. [CrossRef]
52. Abed Abud, A. et al. [DUNE Collaboration] The DUNE Far Detector Vertical Drift Technology, Technical Design Report. *arXiv* **2023**, arXiv:2312.03130.
53. Abed Abud, A. et al. [DUNE Collaboration] Deep Underground Neutrino Experiment (DUNE) Near Detector Conceptual Design Report. *Instruments* **2021**, *5*, 31. [CrossRef]
54. Ingratta, G. The SAND detector at the DUNE near site. In Proceedings of the 41st International Conference on High Energy Physics (ICHEP2022), Bologna, Italy, 6–13 July 2022. [CrossRef]
55. Amelino-Camelia, G. et al. [KLOE Collaboration] Physics with the KLOE-2 experiment at the upgraded DAϕNE. *Eur. Phys. J. C* **2010**, *68*, 619–681. [CrossRef]
56. Abi, B. et al. [DUNE Collaboration] Long-baseline neutrino oscillation physics potential of the DUNE experiment. *Eur. Phys. J. C* **2020**, *80*, 978. [CrossRef]
57. Hagiwara, K. Physics prospects of future neutrino oscillation experiments in Asia. *Nucl. Phys. B Proc. Suppl.* **2004**, *137*, 84–103. [CrossRef]
58. Abe, K. et al. [HyperKamiokande Coll.] Physics potentials with the second Hyper-Kamiokande detector in Korea. *Prog. Theor. Exp. Phys.* **2018**, *2018*, 063C01. [CrossRef]
59. Alekou, A. et al. [ESSnuSB Collaboration] The European Spallation Source neutrino super-beam conceptual design report. *Eur. Phys. J. Spec. Top.* **2022**, *231*, 3779–3955; Erratum in *Eur. Phys. J. Spec. Top.* **2023**, *232*, 15–16. [CrossRef]
60. Alekou, A. et al. [ESSnuSB Collaboration] The ESSnuSB Design Study: Overview and Future Prospects. *Universe* **2023**, *9*, 347. [CrossRef]
61. Capozzi, F.; Giunti, C.; Ternes, C.A. Improved sensitivities of ESSνSB from a two-detector fit. *J. High Energy Phys.* **2023**, *4*, 130. [CrossRef]
62. Longhin, A.; Ludovici, L.; Terranova, F. A novel technique for the measurement of the electron neutrino cross section. *Eur. Phys. J. C* **2015**, *75*, 155. [CrossRef]
63. Acerbi, F. et al. [ENUBET Collaboration] Design and performance of the ENUBET monitored neutrino beam. *Eur. Phys. J. C* **2023**, *83*, 964. [CrossRef]
64. Alsharoa, M.M. et al. [Muon Collaboration] Recent Progress in Neutrino Factory and Muon Collider Research within the Muon Collaboration. *Phys. Rev. ST Accel. Beams* **2003**, *6*, 081001. [CrossRef]
65. Delahaye, J.P.; Diemoz, M.; Long, K.; Mansoulié, B.; Pastrone, N.; Rivkin, L.; Schulte, D.; Skrinsky, A.; Wulzer, A. Muon Colliders. *arXiv* **2019**, arXiv:1901.06150. arXiv:physics.acc-ph/1901.06150.
66. Geer, S. Neutrino beams from muon storage rings: Characteristics and physics potential. *Phys. Rev. D* **1998**, *57*, 6989–6997; Erratum in *Phys. Rev. D* **1999**, *59*, 039903. [CrossRef]
67. De Rujula, A.; Gavela, M.B.; Hernandez, P. Neutrino oscillation physics with a neutrino factory. *Nucl. Phys. B* **1999**, *547*, 21–38. [CrossRef]
68. Choubey, S. et al. [IDS-NF Collaboration] International Design Study for the Neutrino Factory, Interim Design Report. *arXiv* **2011**, arXiv:1112.2853. arXiv:hep-ex/1112.2853.
69. Bogomilov, M. et al. [MICE Collaboration] Demonstration of cooling by the Muon Ionization Cooling Experiment. *Nature* **2020**, *578*, 53–59. [CrossRef] [PubMed]
70. Kyberd, P. et al. [NuSTORM Collaboration] νSTORM - Neutrinos from STORed Muons: Letter of Intent. *arXiv* **2012**, arXiv:1206.0294. arXiv:hep-ex/1206.0294.